APPLIED GEOPHYSICS, Vol.14, No.2 (June 2017), P. 270–278, 6 Figures.
DOI:10.1007/s11770-017-0623-z

# Hybrid absorbing boundary condition for three-dimensional elastic wave modeling*

Liu Xin♦[1,2], Liu Yang[1,2], Ren Zhi-Ming[3], Cai Xiao-Hui[4], Li Bei[1,2], Xu Shi-Gang[1,2], and Zhou Le-Kai[1,2]

**Abstract**: Edge reflections are inevitable in numerical modeling of seismic wavefields, and they are usually attenuated by absorbing boundary conditions. However, the commonly used perfectly matched layer (PML) boundary condition requires special treatment for the absorbing zone, and in three-dimensional (3D) modeling, it has to split each variable into three corresponding variables, which increases the computing time and memory storage. In contrast, the hybrid absorbing boundary condition (HABC) has the advantages such as ease of implementation, less computation time, and near-perfect absorption; it is thus able to enhance the computational efficiency of 3D elastic wave modeling. In this study, a HABC is developed from two-dimensional (2D) modeling into 3D modeling based on the 1st Higdon one way wave equations, and a HABC is proposed that is suitable for a 3D elastic wave numerical simulation. Numerical simulation results for a homogenous model and a complex model indicate that the proposed HABC method is more effective and has better absorption than the traditional PML method.
**Keywords**: 3D elastic wave equation, hybrid absorbing boundary condition, forward modeling

## Introduction

Seismic wave numerical modeling is a technology used to numerically simulate seismic wave propagation and is the key to reverse time migration and to obtain full waveform inversion. While studying seismic exploration, underground media are always regarded as semi-infinite media. However, numerical simulations are limited by computer memory and require artificial boundaries to truncate the computational domain. Absorbing boundary conditions (ABCs) are therefore necessary to attenuate spurious reflections resulting from artificial boundaries. In this respect, the current and commonly used boundary conditions absorb incident waves in a certain range around boundaries with the aim of ultimately attenuating boundary reflections. Three types of frequently-used ABCs exist, which are described in the following paragraphs.

The first type is a wavefield-prediction-based boundary condition. Clayton and Engquist (1977) proposed a wavefield-prediction-based boundary condition based on

Manuscript received by the Editor March 02, 2017; revised manuscript received June 6, 2017
*This research is supported by the National Natural Science Foundation of China (No. 41474110).
1. State Key Laboratory of Petroleum Resources and Prospecting, China University of Petroleum, Beijing 102249, China.
2. CNPC Key Laboratory of Geophysics Prospecting, China University of Petroleum, Beijing 102249, China.
3. School of Geoscience, China University of Petroleum (East China), Qingdao 266580, China.
4. Institute of Geotechnical Engineering, Nanjing University of Technology, Nanjing 210009, China.
♦Corresponding author: Liu Yang (Email: wliuyang@vip.sina.com)

one way wave equations (OWWEs), and Reynolds (1978) derived another OWWE-based ABC, which is known as the transparent boundary condition. Higdon (1991) and Heidari and Guddati (2006) then employed high-order OWWEs and arbitrarily wide-angle wave equations, respectively, to accurately estimate the incident wavefield in the boundary zone; both enhance the absorption of the wavefield-prediction-based boundary condition. In summary, this type of ABC works well for small angle incident waves but fails with respect to large angle incident waves.

The second type of ABC is the damping boundary condition. Cerjan et al. (1985) proposed the absorption of incident waves by multiplying wavefield values with an exponential damping function in the boundary zone. Sochacki et al. (1987) proposed several types of damping functions, and Liu et al. (2014) developed a double absorbing boundary condition based on the damping boundary condition, aiming to boost its performance. However, although this ABC usually utilizes the exponential damping factor to attenuate incident waves, its absorption is poor and the damping factor is difficult to determine.

The third type of ABC is the perfectly matched layer (PML) boundary condition. Bérenger (1994) proposed the PML boundary condition in an electromagnetic wave simulation, and Chu and Weedon formulated the PML boundary condition using complex coordinate stretching. Collino and Tsogka (2001) subsequently applied the PML boundary to a seismic wavefield simulation in anisotropic media, and Du et al. (2010) used the PML boundary condition in elastic wave reverse time migration. Furthermore, Zhao and Shi (2013) applied the PML boundary condition to an elastic wave numerical simulation in irregular topography model. The PML boundary condition has been widely used because it can absorb incident waves of any angles and frequencies. The traditional PML boundary condition is usually applied to first-order wave equations. However, computational cost and memory storage increases and a proper decay factor needs to be selected to achieve good absorption because the traditional PML boundary condition needs to split each variable into separate variables that are either vertical or parallel to the boundary, and wave equations have to be modified accordingly to include decay factors. Komatitsch and Tromp (2003) applied the PML method to second-order wave equations, this method necessitates splitting of the displacement terms into four terms and 3rd order temporal derivatives need to be calculated; therefore, this method is both inefficient and computationally costly. Furthermore, Bécache et al. (2003) and Festa et al. (2005) showed clearly that the traditional PML boundary condition fails to absorb large angle incident waves. With the aim of improving these disadvantages, many researchers have proposed a nonsplit-PML boundary condition (Martin et al., 2008; Qin et al., 2009; Li et al., 2013). However, although the convolution of the PML boundary condition has better absorption for large angle incident waves, it has to bring in auxiliary variables and is computational costly.

Among the above-mentioned three types of ABCs, the wavefield-prediction-based boundary condition offers moderate computational costs and good absorption. This method generally utilizes OWWEs to predict the wavefield near the boundary and uses two-way wave equations (TWWEs) to calculate the wavefield in the non-absorbing zone. However, the difference between the two types of wave equations results in certain differences between the wavefields computed by two types of wave equations. The wavefield difference is one of the primary causes of strong boundary reflections. To reduce this difference, Liu and Sen (2010) inserted a transition zone between the internal non-absorbing zone and external boundaries and reduced the difference in the transition zone by linearly weighting the OWWE and TWWE wavefield. This HABC has the advantages such as ease of implementation, less computation time, and near-perfect absorption. Chang and Liu then used the HABC in high-order implicit finite-difference numerical modeling, and Ren and Liu (2013) developed the HABC into frequency domain seismic wave numerical modeling. Ren and Liu (2014) subsequently proposed two HABCs for the first-order velocity-stress wave equations based on the 1st and the 2nd Higdon OWWEs and determined that the HABC based on 1st Higdon OWWEs has the advantage over the traditional PML by providing higher efficiency and better absorption. With developments in seismic exploration moving from two-dimensional (2D) survey lines to a three-dimensional (3D) work area, there has been a rapid increase in the amount of research being conducted on finite-difference numerical modeling of 3D seismic waves (Moczo, 2000; Liu and Sen, 2011; Chu and Stoffa, 2012; Cai et al., 2015); therefore, it is considered beneficial to apply the 1st Higdon HABC to 3D elastic wave modeling.

In this study, the 1st Higdon HABC is developed for the 1st order stress-velocity equation of a 3D elastic wave, and the least-square-based global optimal implicit staggered-grid finite-difference scheme is utilized to simulate wave propagation in both a homogenous and complex model. In addition, memory storage, computing time, and absorption of the split-PML boundary condition and the 1st Higdon HABC are all analyzed, and results validate the advantages of using the 1st Higdon HABC in numerical modeling of 3D elastic waves.

# Method

## 3D elastic wave equation and high order finite-difference method

The 3D elastic wave equations in homogenous isotropic media are expressed by (Graves, 1996)

$$\frac{\partial \sigma_{xx}}{\partial t} = \lambda\left(\frac{\partial v_x}{\partial x} + \frac{\partial v_y}{\partial y} + \frac{\partial v_z}{\partial z}\right) + 2\mu\frac{\partial v_x}{\partial x}, \frac{\partial \tau_{xz}}{\partial t} = \mu\left(\frac{\partial v_x}{\partial z} + \frac{\partial v_y}{\partial x}\right), \rho\frac{\partial v_x}{\partial t} = \frac{\partial \tau_{xx}}{\partial x} + \frac{\partial \sigma_{xy}}{\partial y} + \frac{\partial \tau_{xz}}{\partial z}, \tag{1a}$$

$$\frac{\partial \sigma_{yy}}{\partial t} = \lambda\left(\frac{\partial v_x}{\partial x} + \frac{\partial v_y}{\partial y} + \frac{\partial v_z}{\partial z}\right) + 2\mu\frac{\partial v_y}{\partial y}, \frac{\partial \tau_{xy}}{\partial t} = \mu\left(\frac{\partial v_x}{\partial y} + \frac{\partial v_y}{\partial x}\right), \rho\frac{\partial v_y}{\partial t} = \frac{\partial \tau_{yx}}{\partial x} + \frac{\partial \sigma_{yy}}{\partial y} + \frac{\partial \tau_{yz}}{\partial z}, \tag{1b}$$

$$\frac{\partial \sigma_{zz}}{\partial t} = \lambda\left(\frac{\partial v_x}{\partial x} + \frac{\partial v_y}{\partial y} + \frac{\partial v_z}{\partial z}\right) + 2\mu\frac{\partial v_z}{\partial z}, \frac{\partial \tau_{yz}}{\partial t} = \mu\left(\frac{\partial v_z}{\partial y} + \frac{\partial v_y}{\partial z}\right), \rho\frac{\partial v_z}{\partial t} = \frac{\partial \tau_{zx}}{\partial x} + \frac{\partial \tau_{zy}}{\partial y} + \frac{\partial \sigma_{zz}}{\partial z}, \tag{1c}$$

where in $(v_x, v_y, v_z)$ represents particle velocity, ($\sigma_{xx}$, $\sigma_{yy}$, $\sigma_{zz}$, $\tau_{xy}$, $\tau_{xz}$, $\tau_{yx}$) represents particle stress, $\rho$ represents density, and ($\lambda$, $\mu$) represent Lamé constants.

The high-order staggered-grid finite-difference method is used to calculate equation (1) (Virieux, 1984 and 1986).

Generally, the second-order central-difference scheme is used to calculate temporal derivatives; for example, the temporal derivative of $v_x$ is expressed by (e.g., Dong, 2000)

$$\frac{\partial v_x}{\partial t} = \frac{v_{x_{i,j,l}}^{t+0.5} - v_{x_{i,j,l}}^{t-0.5}}{\Delta t}. \tag{2}$$

For spatial derivatives, the least-square-based global optimal implicit staggered-grid finite-difference scheme is generally utilized. For example, the spatial derivative of $v_x$ in the $x$-direction can be written as (Liu and Sen, 2009; Liu, 2014)

$$\frac{\partial v_{x_{i-1,j,l}}}{\partial x} + a\frac{\partial v_{x_{i,j,l}}}{\partial x} + \frac{\partial v_{x_{i+1,j,l}}}{\partial x} \approx \frac{1}{h}\sum_{m=1}^{M} c_m [v_{x_{i+m-0.5,j,l}} - v_{x_{i-m+0.5,j,l}}], \tag{3}$$

and the corresponding constants in equation (3) can be estimated using the following equations

$$a = \sum_{m=1}^{M}(2m-1)c_m - 2, \tag{4}$$

$$\phi_m(\beta) = \sin[(m-0.5)\beta] - (m-0.5)\beta, f(\beta) = (\cos\beta - 1)\beta, \beta = kh, \tag{5}$$

$$\sum_{m=1}^{M}[\int_0^b \phi_m(\beta)\phi_n(\beta)d\beta]c_m = \int_0^b f(\beta)\phi_n(\beta)d\beta, (n = 1, 2, ..., M), \tag{6}$$

where in ($i$, $j$, $l$) and $t$ are the spatial and temporal coordinates, respectively; $h$ and $\Delta t$ are the temporal and spatial interval, respectively; $M$ is the FD operator length; and k is the wavenumber.

The corresponding error of the dispersion relation for the spatial derivatives calculated using this method is (Liu and Sen, 2009; Liu, 2014)

$$\varepsilon(\beta) = \frac{2\sum_{m=1}^{M} c_m \sin[(m-0.5)\beta]}{(a + 2\cos\beta)} - 1. \tag{7}$$

If the spatial derivative of $v_x$ in the $x$-direction is used as an example, the three steps used to implement the least-square-based global optimal implicit staggered-grid finite-difference scheme are as follows:

(1) Substitute equation (5) into equations (6) and (4) to obtain the finite-difference coefficients, $c_m$ and $a$.

(2) Substitute $c_m$ and $a$ into equation (7). If the error reaches the defined requirement, proceed to next step; if not, return to the previous step and adjust the

wavenumber range or the FD operator length.

(3) Substitute $c_m$ and $a$ into equation (3) to obtain a linear system of equations and then calculate the spatial derivative of $v_x$ in the $x$-direction on all grids. Finally, use the computed spatial derivatives and temporal derivatives to calculate equation (1).

Hybrid absorbing boundary condition for 3D elastic wave equations

The HABC is extended to 3D modeling, as shown in Figure 1. Corresponding 3D Higdon OWWEs are expressed by

$$\begin{bmatrix} Q_1 & 0 & 0 & 0 & 0 & 0 & 0 & 0 & 0 \\ 0 & Q_1 & 0 & 0 & 0 & 0 & 0 & 0 & 0 \\ 0 & 0 & Q_1 & 0 & 0 & 0 & 0 & 0 & 0 \\ 0 & 0 & 0 & Q_1 & 0 & 0 & 0 & 0 & 0 \\ 0 & 0 & 0 & 0 & Q_1 & 0 & 0 & 0 & 0 \\ 0 & 0 & 0 & 0 & 0 & Q_1 & 0 & 0 & 0 \\ 0 & 0 & 0 & 0 & 0 & 0 & Q_1 & 0 & 0 \\ 0 & 0 & 0 & 0 & 0 & 0 & 0 & Q_1 & 0 \\ 0 & 0 & 0 & 0 & 0 & 0 & 0 & 0 & Q_1 \end{bmatrix} \mathbf{u} = 0, \quad (8)$$

where in $\mathbf{u} = [v_x, v_y, v_z, \sigma_{xx}, \sigma_{yy}, \sigma_{yy}, \tau_{xy}, \tau_{xz}, \tau_{yz}]^T$, and $Q_1$ is dependent on boundary types.

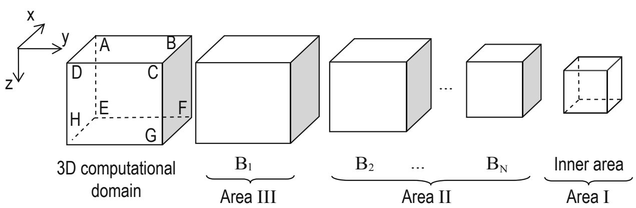


**Fig.1 Illustration of 1st Higdon HABC for 3D elastic wave numerical simulation (Liu and Sen, 2011).**

For each layer of the absorbing boundary it is necessary to consider six boundary surfaces, 12 boundary edges, and eight boundary apexes. The discretization schemes proposed by Higdon (1991) are used to calculate the OWWEs. In addition, if the 1st Higdon HABC for the particle velocity, $v_x$, in the x-direction is different at the boundary surfaces, edges, and apexes, it is then described separately.

## Boundary surfaces

If the boundary surface normal to the negative x-direction ($\Omega_{DCGH}$ in Figure 1) is taken as an example, the 1st Higdon HABC can be illustrated for $v_x$ on the boundary surface. At $\Omega_{DCGH}$, $Q_1$ can be expressed by

$$Q_1 = (\beta \frac{\partial}{\partial t} - v_p \frac{\partial}{\partial x}), \quad (9)$$

where in $\beta = (1 + v_p / v_s)/2$, ($v_p$, $v_s$) are P-wave and S-wave velocities, respectively.

The OWWEs discretization scheme for $v_x$ is (Higdon, 1994)

$$v_{x_{i,j,l}}^{t+0.5} = -q_x v_{x_{i+1,j,l}}^{t+0.5} - q_t v_{x_{i,j,l}}^{t-0.5} - q_{xt} v_{x_{i+1,j,l}}^{t-0.5}, \quad (10)$$

and the coefficients in this equation can be expressed by

$$q_x = \frac{b(\beta + r) - r}{(\beta + r)(1 - b)}, \quad (11a)$$

$$q_t = \frac{b(\beta + r) - \beta}{(\beta + r)(1 - b)}, \quad (11b)$$

$$q_{xt} = \frac{b}{b - 1}, \quad (11c)$$

where in $r = \frac{v_p \Delta t}{h}$ and $b$ is a constant ranging from 0.3 to 0.5.

## Boundary edges

Taking the boundary edges ($L_{DC}$ in Figure 1) as an example (which are the intersection line of the boundary normal to the negative x-direction ($\Omega_{DCGH}$ in Figure 1) and the boundary normal to the negative $y$-direction ($\Omega_{ABCD}$ in Figure 1), the 1st Higdon HABC is illustrated for $v_x$ on the boundary edge.

Higdon (1994) showed that OWWEs expressed by equation (10) can perfectly absorb the incident wave propagating in the $x$-direction. Therefore, the discretization scheme of the boundary condition for $L_{DC}$ can be obtained by taking the weighted average of the discretization schemes of the two absorbing boundary surfaces. The discretization scheme for $L_{DC}$ can be expressed by

$$v_{x_{i,j,l}}^{t+0.5} = -0.5 q_x (v_{x_{i+1,j,l}}^{t+0.5} + v_{x_{i,j+1,l}}^{t+0.5}) \\ -q_t v_{x_{i,j,l}}^{t-0.5} - 0.5 q_{xt} (v_{x_{i+1,j,l}}^{t-0.5} + v_{x_{i,j+1,l}}^{t-0.5}). \quad (12)$$

## Boundary apexes

The boundary apex ($P_D$ in Figure 1) is used as an example, which includes the cross-point of the boundary normal to the negative $x$-direction ($\Omega_{DCGH}$ in Figure 1), the boundary normal to the negative y-direction ($\Omega_{ABCD}$ in Figure 1) and the boundary normal to the negative z-direction ($\Omega_{ADHE}$ in Figure 1). The 1st Higdon HABC is illustrated here for $v_x$ at the boundary apex.

To attenuate incident waves from all angles, it is assumed that the incident wave at $P_D$ in Figure 1 has equal angles between the *x*-direction, *y*-direction, and *z*-direction. Therefore, the discretization scheme for the boundary condition of $P_D$ can be obtained by taking the weighted average of the discretization schemes of the three absorbing boundary surfaces. The discretization scheme for $P_D$ can be expressed by

$$v_{x_{i,j,l}}^{t+0.5} = -q_x(v_{x_{i+1,j,l}}^{t+0.5} + v_{x_{i,j+1,l}}^{t+0.5} + v_{x_{i,j,l+1}}^{t+0.5})/3 \\ -q_t v_{x_{i,j,l}}^{t-0.5} - q_{xt}(v_{x_{i+1,j,l}}^{t-0.5} + v_{x_{i,j+1,l}}^{t-0.5} + v_{x_{i,j,l+1}}^{t-0.5})/3. \quad (13)$$

The 1st Higdon HABC utilized in this study divides the computing domain into three parts. The parts (from the outside inwards) are as follows: the boundary (Area II, $B_1$), transition zone (Area III, $B_2$ to $B_N$), and inner area (Area I, non-absorbing zone), as shown in Figure 1. Implementation of the 1st Higdon HABC is conducted as follows:

(1) Wavefield values, $\mathbf{u}^{\mathbf{two}}$, within Areas I and II are calculated by equation (1);

(2) Wavefield values, $\mathbf{u}^{\mathbf{one}}$, within Areas II and III are calculated by equations (10), (12), and (13);

(3) Wavefield values within Area II are weighted using $\mathbf{u}_{B_i} = (1-w_{B_i})\mathbf{u}_{B_i}^{\mathbf{one}} + w_{B_i}\mathbf{u}_{B_i}^{\mathbf{two}}$ and $w_{B_i} = (i-1)/N$, $i$ = 2, 3, …, $N$ wherein subscript $B_i$ indicates the variables of the ith layer and $w_{B_i}$ is a weight that varies from 0 to 1 from Area III to Area I, so that $\mathbf{u}_i = \mathbf{u}_i^{one}$ at Area III and $\mathbf{u}_i = \mathbf{u}_i^{two}$ at the boundary of Area I.

If $N$ = 1, it can thus be seen that Area II vanishes and the 1st Higdon HABC degenerates to the OWWEs boundary condition.

# Forward modeling examples

To analyze the effectiveness and superiority of the 1st Higdon HABC, the memory storage of the split-PML boundary condition and the 1st Higdon HABC are compared. In addition, the split-PML method and the 1st Higdon HABC are applied to a numerical simulation of seismic wave propagation in a homogenous model and in the SEG/EAGE salt model. The $N$-layer HABC and $L_{PML}$-layer PML method ($N = L_{PML} = 10$) are used to absorb artificial boundary reflections and the absorption and computing time are compared. Magnitudes of information pertaining to the snapshots and seismic records in this study are uniformly $10^{-10}$.

Occupied memory at boundary zone

As shown in Table 1, the split-PML method has to split each variable into three separate variables in the absorbing zone; therefore, wavefields belonging to as many as 18 variables need be stored. However, it is not necessary for the 1st Higdon HABC to split any variables, and thus the wavefields of only six variables need be stored. Consequently, the use of the 1st Higdon HABC saves a large amount of computer memory when its thickness, $N$, is equal to the $L_{PML}$, which is the thickness of the split-PML method.

**Tabel 1 Stored variables of two types of absorbing boundary conditions**

| Absorbing boundary condition | Stored variables |
|---|---|
| PML boundary condition | $v_x^x, v_x^y, v_x^z, v_y^x, v_y^y, v_y^z, v_z^x, v_z^y, v_z^z, \sigma_{xx}^x, \sigma_{xx}^y, \sigma_{xx}^z, \sigma_{yy}^x, \sigma_{yy}^y, \sigma_{yy}^z, \sigma_{zz}^x, \sigma_{zz}^y, \sigma_{zz}^z, \tau_{xy}^x, \tau_{xy}^y, \tau_{xy}^z, \tau_{xz}^x, \tau_{xz}^y, \tau_{xz}^z, \tau_{yz}^x, \tau_{yz}^y, \tau_{yz}^z$ |
| 1st Higdon HABC | $v_x, v_y, v_z, \sigma_{xx}, \sigma_{yy}, \sigma_{zz}, \tau_{xy}, \tau_{xz}, \tau_{yz}$ |

## Homogenous model

The P- and S-wave velocities of the homogenous model are 3480 m/s and 2420 m/s, respectively. The model dimension is 1000 m × 1000 m × 1000 m, with a grid size of $h$ = 10 m and a temporal sampling rate of $\tau$ = 1 ms. An 18-Hz Ricker wavelet located at the model's center is applied to the *x*-component of particle velocity, and a receiver is located at (150 m, 200 m, 100 m). Figure 2a, 2d, and 2g show snapshots obtained when no absorbing boundary is used and the 1st Higdon HABC and split-PML boundary condition. Figure 3 shows the corresponding seismic records wherein the survey line is located at $x$ = 0 m–1000 m, $y$ = 500 m, and $z$ = 10 m. Table 2 shows the computing times of the simulating wave propagating for 900 ms using the different boundary conditions. In addition, Figure 4 shows the seismic waveforms observed at the receiver (150 m, 200 m, 100 m) using the different boundary conditions and the residual waveforms between the observed waveforms and the reference waveform; these are obtained by extending the homogenous model so that it is large enough to avoid artificial boundary reflections. The computer used is a ThinkPad with an Intel(R) Core(TM) i7-4790 CPU @ 3.6 GHz.

The following are shown in Figures 2, 3, 4, 5, and Table 2:

(1) artificial boundary reflections of the P- and S-wave

are almost attenuated by the 1st Higdon HABC (Figure 2d, 2e, and 2f) and the split-PML boundary condition (Figures 2g, 2h, and 2i), respectively;

(2) the 1st Higdon HABC (Figure 3a) has a better absorption than the split-PML boundary condition (Figure 3b);

(3) the three components of the observed seismic waveforms (Figure 4) indicate that the 1st Higdon HABC has better absorption than that of the split-PML boundary condition;

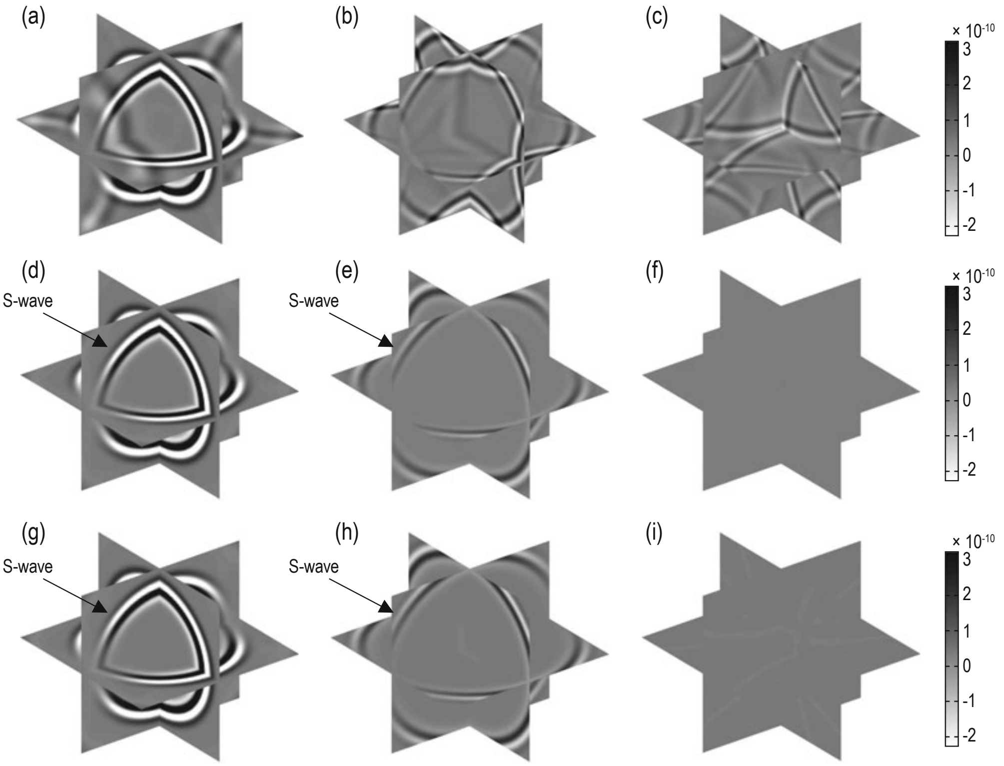


**Fig.2 Elastic wave snapshots of homogenous model: (a), (b), and (c) are 3D snapshots at 280 ms, 400 ms and 600 ms, respectively, wherein no boundary condition is used; (d), (e), and (f) are 3D snapshots at 280 ms, 400 ms, and 600 ms, respectively, using the 1st Higdon HABC; and (g), (h), and (i) are 3D snapshots at 280 ms, 400 ms, and 600 ms, respectively, using the split-PML boundary condition.**

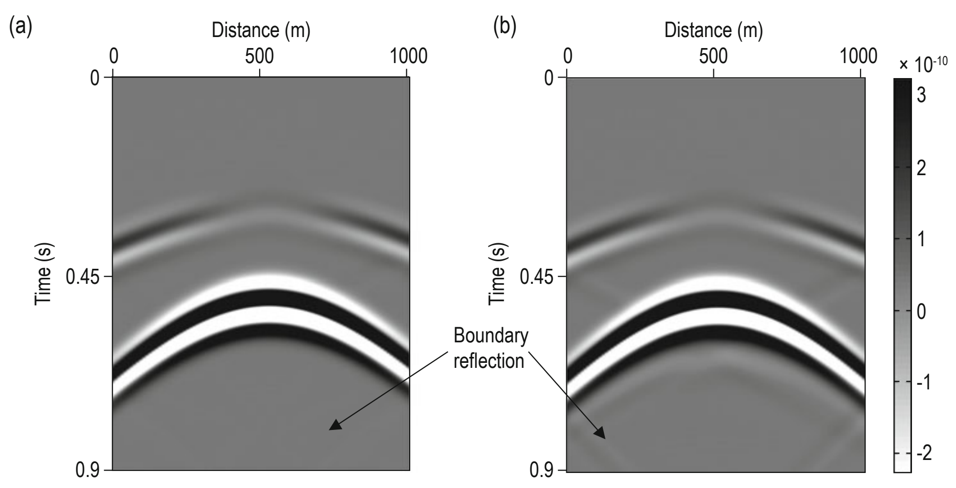


**Fig.3 Elastic wave seismic records of homogenous model: (a) and (b) are seismic records obtained using the 1st Higdon HABC and the split-PML boundary condition, respectively.**

(4) Table 2 shows that the 1st Higdon HABC takes less time than the split-PML boundary condition to conduct the numerical simulation; in particular, it enhances the computational efficiency by approximately 20% for this homogenous model.

**Table 2 Computing times used in homogenous model numerical simulation using different boundary conditions**

| Absorbing boundary condition | CPU time (s) |
|---|---|
| PML boundary condition | 2436 |
| 1st Higdon HABC | 1938 |

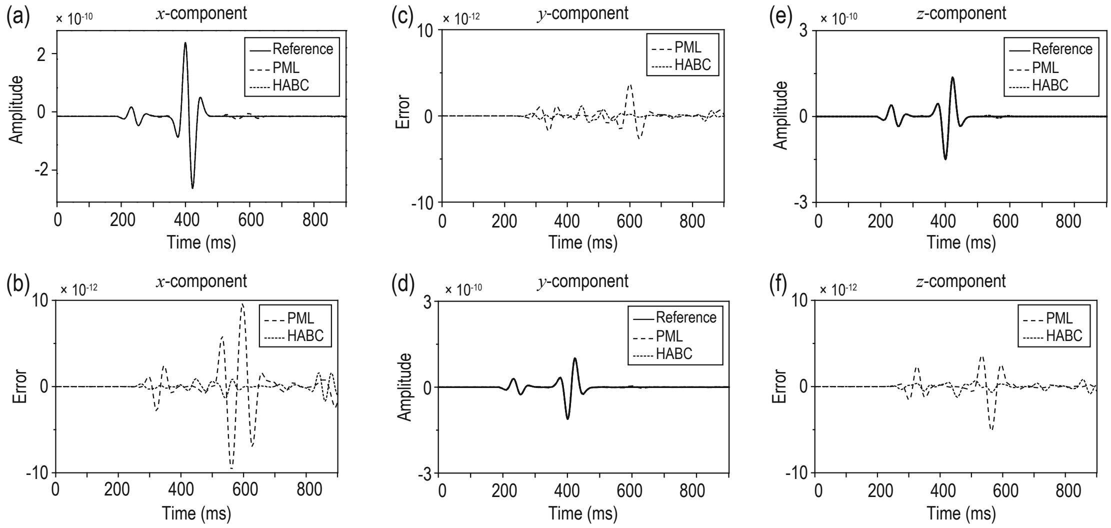


**Fig.4 Seismic waveforms obtained using different boundary conditions at the receiver (150 m, 200 m, 100 m) and residual waveforms between the observed waveforms and the reference waveform. The reference waveform is obtained by extending the model so that it is large enough to avoid artificial boundary reflections. (a), (c) and (e) show the three components of the observed waveforms; and (b), (d) and (f) show the three components of the residual waveforms between the observed and the reference.**

## SEG/EAGE salt model

An elastic wave numerical simulation is performed for part of the 3D SEG/EAGE salt model. Figure 5 shows the P-wave velocity, and the corresponding density and S-wave velocity are computed using empirical formulas. The model has a dimension of 1500 m × 1500 m × 1500 m, grid size of $h$ = 10 m, and temporal sampling rate of $\tau$ = 0.5 ms. An 18-Hz Ricker is located at the top of the

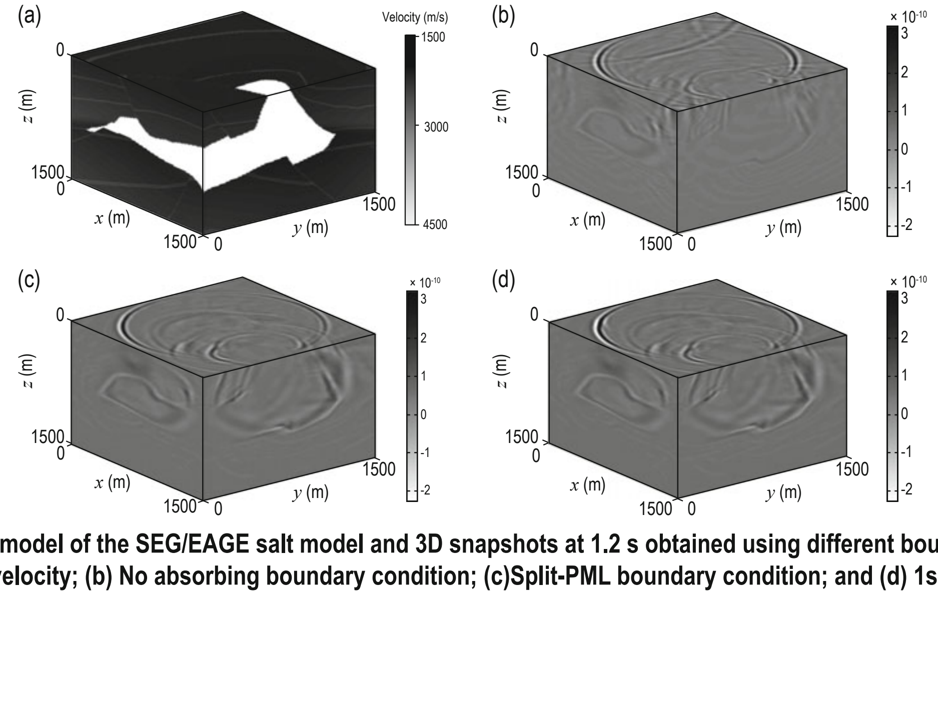


**Fig.5 Velocity model of the SEG/EAGE salt model and 3D snapshots at 1.2 s obtained using different boundary conditions: (a) P-wave velocity; (b) No absorbing boundary condition; (c)Split-PML boundary condition; and (d) 1st Higdon HABC.**

model (750 m, 750 m, 20 m) to generate an explosive energy source. The survey line is located at $x$ = 0 m–1500 m, $y$ = 750 m, and $z$ = 10 m. Figures 5b, 5c, and 5d show 1.2 s snapshots obtained using no absorbing boundary condition and the 1st Higdon HABC and split-PML boundary condition.

The dashed box in Figure 6a shows the artificial boundary reflections obtained when no boundary condition is used. In addition, as shown in Figure 6b and 6c, although both boundary conditions have good absorption, the dashed boxes indicate that the 1st Higdon HABC has better absorption than the split-PML boundary condition.

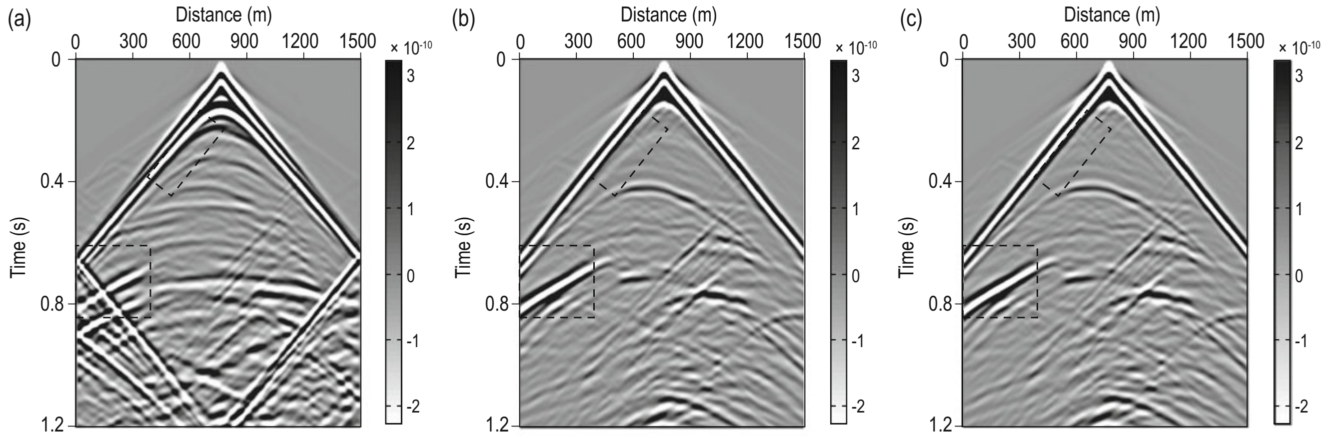


**Fig.6 Seismic records obtained using different boundary conditions: (a) no absorbing boundary condition; (b) 1st Higdon HABC; and (c) split-PML boundary condition.**

## Conclusions

The 1st Higdon HABC is extended from a 2D to 3D elastic wave equation, and the least-square-based global optimal staggered-grid finite-difference method is employed in numerical modeling. The computing time, memory storage, and absorption of the 1st Higdon HABC and the split-PML boundary condition are compared. Results indicate that the 1st Higdon HABC has advantages such as less computing time, requirement of less memory storage, and enablement of better absorption in 3D forward modeling. Therefore, the 1st Higdon HABC is considered capable of enhancing the efficiency of reverse time migration and full waveform inversion.

## References

Bécache, E., Fauqueux, S., and Joly P., 2003, Stability of perfectly matched layers, group velocities and anisotropic waves: Journal of Computational Physics, **188**(2), 399–433.

Bérenger, J. P., 1994, A perfectly matched layer for the absorption of electromagnetic waves: Journal of Computational Physics, **114**(2), 185–200.

Cai, X., Liu, Y., Ren, Z., Wang, J., Chen, Z., Chen, K., and Wang, C., 2015, Three-dimensional acoustic wave equation modeling based on the optimal finite-difference scheme: Applied Geophysics, **12**(3), 409–420.

Cerjan, C., Kosloff, D., Kosloff, R., and Resef, M., 1985, A nonreflecting boundary condition for discrete acoustic and elastic wave equations: Geophysics, **50**(4), 705–708.

Chang S., and Liu Y., 2013, A truncated implicit high-order finite-difference scheme combined with boundary conditions: Applied Geophysics, **10**(1), 53–62.

Chew, W. C., and Weedon, W. H., 1994, A 3-D perfectly matched medium from modified Maxwell's equations with stretched coordinates: Microwave and Optical Technology Letters, **7**(13), 599 – 604

Chu, C., and Stoffa, P., 2012, Efficient 3D frequency response modeling with spectral accuracy by the rapid expansion method: Geophysics, **77**(4), T117–T123.

Clayton, C., and Engquist, B., 1977, Absorbing boundary conditions for acoustic and elastic wave equations: Bulletin of the Seismological Society of America, **67**(6), 1529–1540.

Collino, R., and Tsogka, C., 2001, Application of the perfectly matched absorbing layer model to the linear elastodynamic problem in anisotropic heterogeneous media: Geophysics, **66**(1), 294–307.

Dong, L., Ma, Z., and Cao, J., 2000, A staggered-grid high-order difference method of one-order elastic wave equation: Chinese Journal of Geophysics, **43**(3), 411–419.

Du, Q., Sun, R., Qin, T., Zhu, Y., and Bi, L., 2010, A study of perfectly matched layers for joint multi-component reverse-time migration: Applied Geophysics, **7**(2), 166–173.

Festa, G., Delavaud, E., and Vilotte, J. P., 2005, Interaction between surface waves and absorbing boundaries for wave propagation in geological basins: 2D numerical simulations, Geophysics Research Letters, **32**(20), 55–102.

Graves, R. W., 1996, Simulating seismic wave propagation in 3D elastic media using staggered-grid finite-difference: Bulletin of the Seismological Society of America, **86**(4), 1091–1160.

Heidari, A. H., and Guddati, M. N., 2006, Highly accurate absorbing boundary conditions for wide-angle wave equations: Geophysics, **71**(3), S85–S97.

Higdon, R. L., 1991, Absorbing boundary conditions for elastic waves: Geophysics, **56**(2), 231–241.

Komatitsch, D., and Martin, R., 2009, An unsplit convolutional perfectly matched layer technique improved at grazing incidence for the viscoelastic wave equation: Geophysics Journal International, **179**(1), 146–153.

Komatitsch, D., and Tromp, J., 2003, A perfectly matched layer absorbing boundary condition for the second-order seismic wave equation: Geophysics Journal International, 154(1), 146–153.

Li, Z., Tian, K., Huang, J., Cao, X., Li, N., and Li, Q., 2013, An unsplit implementation of the multi-axial perfectly matched layer: Progress in Geophysics, **28**(6), 2984–2992.

Liu, Y., and Sen, M. K., 2009, An implicit staggered-grid finite-difference method for seismic modeling, Geophysics Journal International, **179**(1), 459–474.

Liu, Y., 2014, Optimal staggered-grid finite-difference schemes based on least-squares for wave equation modelling: Geophysical Journal International, **197**(2), 1033–1047.

Liu, Y., Li, X., and Chen, S., 2014, Application of the double absorbing boundary condition in seismic modeling: Applied Geophysics, **11**(4), 111–119.

Liu, Y., and Sen, M. K., 2010, A hybrid scheme for absorbing edge reflections in numerical modeling of wave propagation: Geophysics, **75**(2), A1–A6.

Liu, Y., and Sen, M. K., 2011, 3D acoustic wave modeling with time-space domain dispersion-relation-based finite-difference schemes and hybrid absorbing boundary conditions: Exploration Geophysics, **42**(3), 176–189.

Martin, R., Komatitsch, D., and Gedney, S. D., 2008, A variational formulation of stabilized unsplit convolutional perfectly matched layer for the isotropic or anisotropic seismic wave equations: Computing Modeling in Engineering and Science, **37**(3), 274–304.

Moczo, P., Kristek, J., and Halada, L., 2000, 3D fourth-order staggered-grid finite-difference schemes: Stability and grid dispersion: Bulletin of the Seismological Society of America, **90**(3), 587–603.

Qin, Z., Lu, M., Zheng, X., Yao, Y., Zhang, C., and Song, J., 2009, The implementation of an improved NPML absorbing boundary condition in elastic wave modeling: Applied Geophysics, **6**(2), 113–121.

Ren, Z., and Liu, Y., 2013, A hybrid absorbing boundary condition for frequency-domain finite-difference modeling: Journal of Geophysics and Engineering, **10**(5), 054003 (16pp).

Ren, Z., and Liu, Y., 2014, Numerical modeling of the first order elastic equations with the hybrid absorbing boundary condition: Chinese Journal of Geophysics, **57**(2), 595–606.

Reynolds, A. C., 1978, Boundary conditions for the numerical solution of wave propagation problems: Geophysics, **43**(6), 1099–1110.

Sochacki, J., Kubichek, R., George, J., Fletcher, W., and Smithson, S., 1987, Absorbing boundary conditions and surface waves: Geophysics, **52**(1), 60–71.

Virieux, J., 1984, SH-wave propagation in heterogeneous media: velocity-stress finite-difference method: Geophysics, **49**(11), 1933–1942.

Virieux, J., 1986. P-SV wave propagation in heterogeneous media: velocity stress finite difference method: Geophysics, **51**(4), 889–901.

Wang, T., and Tang, X., 2003, Finite-difference modeling of elastic wave propagation: A nonsplitting perfectly matched layer approach: Geophysics, **68**(5), 1749–1755.

Zhao, J., and Shi, Q., 2013, Perfectly matched layer-absorbing boundary condition for finite-element time-domain modeling of elastic wave equations: Applied Geophysics, **10**(3), 323–326.

**Liu Xin**, he received a bachelor's degree from China University of Petroleum (Beijing) (2015) and is now a master student in China University of Petroleum (Beijing). His research interests include seismic wave equation numerical modeling and migration.